

Edge and Central Cloud Computing: A Perfect Pairing for High Energy Efficiency and Low-latency

Xiaoyan Hu, *Student Member, IEEE*, Lifeng Wang, *Member, IEEE*,
Kai-Kit Wong, *Fellow, IEEE*, Yangyang Zhang, Zhongbin Zheng, and
Meixia Tao, *Senior Member, IEEE*

Abstract

In this paper, we study the coexistence and synergy between edge and central cloud computing in heterogeneous cellular networks (HetNets), in which multi-antenna small base stations (SBSs) empowered by clouds at the edge offer computing services for user equipments (UEs), whereas a macro base station (MBS) provides computing services from a central cloud via a high-speed backhaul. With processing latency constraints at the edge cloud and backhaul, we aim to minimize the network energy consumption (the energy used for task offloading as well as computation) through jointly optimizing the cloud selection, the UE's transmit power, the SBS's receive beamformer, and the SBS's transmit covariance matrix. We devise a tractable solution that can achieve great performance gain over conventional schemes. With large-scale antennas at the MBS, the massive multiple-input multiple-output (MIMO) backhaul can significantly reduce the complexity of our algorithm and obtain even better performance.

Index Terms

Edge computing, central cloud computing, HetNets, backhaul, massive MIMO.

X. Hu, L. Wang and K.-K. Wong are with the Department of Electronic and Electrical Engineering, University College London, London WC1E 7JE, UK (Email: {xiaoyan.hu.16, lifeng.wang, kai-kit.wong}@ucl.ac.uk).

Y. Zhang is with the Kuang-Chi Institute of Advanced Technology, Shenzhen 518057, China (Email: yangyang.zhang@kuang-chi.org).

Z. Zheng is with the East China Institute of Telecommunications, China Academy of Information and Communications Technology, Shanghai 200001, China (Email: ben@ecit.org.cn).

M. Tao is with the Department of Electronic Engineering, Shanghai Jiao Tong University, Shanghai 200240, China (Email: mxtao@sjtu.edu.cn).

I. INTRODUCTION

A. *Motivation and Prior Works*

Edge computing is regarded as one of the key enablers to shape the future intelligent wireless networks. The rationale behind edge computing is that cloud computing can be carried out at the edge of wireless networks, to offload computing tasks of user equipment (UE) and prolong their battery lifetime [1, 2]. The standardization bodies and industry associations such as ETSI and 5GAA have identified various edge computing use cases for 5G cellular, vehicle-to-everything (V2X) and massive machine-type communications (mMTC) [3, 4].

For practical deployment, several edge computing architectures have already been proposed such as mobile edge computing (MEC) [5], fog computing [6, 7], and also cloudlets [8]. MEC allows base stations (BSs) to have the ability of storage and processing, to guarantee that UEs are directly connected to the edge clouds. Fog computing is a more flexible computing architecture consisting of highly heterogeneous fog computing nodes (FCNs) with different levels of computing ability such as routers and network gateways. In wireless local area networks (Wi-Fi access), cloudlets run virtual machines and the computing resources allocated to cloudlets are managed by cloudlet agents [8]. Recently, multi-access edge computing (also using the same acronym “MEC” originated from mobile edge computing) has been introduced to support multiple access technologies including cellular, Wi-Fi, etc. [9]

Considerable attention has been paid to the design and analysis of edge computing in cellular networks, e.g., [10–14]. The tradeoff between energy consumption and latency in information transmission and computation stages is analyzed in [10], where an energy-limited UE offloads the application tasks to a small BS (SBS) for processing. In [11], a multi-user computation offloading problem is considered in a single-cell scenario and game-theoretical solutions are proposed in order to maximize the cell load and minimize the cost in terms of computational time and energy. Later in [12], time and frequency allocation problems for improving energy efficiency are studied by considering multi-user computation offloading in a single cell equipped with limited cloud capacity, where an offloading priority function is derived to accommodate users’ priorities. The work of [13] examines a single-cloudlet scenario where multiple UEs are served with equal-time sharing, and a successive convex optimization approach is developed to minimize the network energy consumption under a computing latency constraint. Recent works also focus on multi-service scenarios where BSs are capable of computing and caching. For

example, [14] studies a single MEC server with storage capability and aims to maximize the revenue of providing these services by optimizing computation offloading decision, resource allocation, and content placement strategy.

Since Internet-of-Things (IoT) devices may lack computing capability, edge computing can achieve local execution, which avoids the frequent delivery of massive computing tasks to the core networks with central cloud for computing, and thus reduces the computing latency and backhaul congestion. The survey work [15] presents a comprehensive overview of fog computing in IoT networks and illustrates how fog computing tackles the challenges in IoT. In [16], Lyapunov optimization techniques are adopted to develop an online MEC scheduling solution with partial knowledge of IoT network.

The implementation of edge computing in energy harvesting networks can further reduce the conventional grid power consumption by renewable energy harvesting or prolong the devices' lifetime through wireless energy harvesting. In [17], BSs are powered by hybrid energy supplies including green energy and grid power, and a green-energy aware cloudlet solution is proposed to minimize the total grid power consumption. Recent works such as [18–21] consider edge computing in RF energy harvesting networks. In [18], a single-antenna sensor harvests RF energy from a dedicated BS for computation offloading, and the CPU frequency for each required CPU cycle is optimized. In [19], two single-antenna UEs are powered by a single-antenna access point (AP) and one of the UEs is selected to act as a relay to help offload the far-away UE's computation tasks so as to satisfy the latency constraint as well as reduce the total energy consumption of the AP. Also, the work of [20] assumes that a multi-antenna AP delivered RF energy to several single-antenna UEs, and computing tasks are jointly executed by the AP and UEs. Their problem is to minimize the AP's energy consumption while successful processing is guaranteed. Unlike the considered network in [20] where wireless power transfer and computation offloading are operated over orthogonal frequency bands, the work [21] designs a new time frame that the AP first broadcasts the RF energy and then the energy-constrained UEs offload their tasks to the AP at their allocated time slots.

B. Our Contributions

The aforementioned works mainly concentrate on small-scale edge computing networks such as the single MEC server or cloudlet case [11–14, 16, 18–21]; however, edge computing cannot replace entirely the present central cloud computing, due to the fact that edge computing is set to

push limited processing and storage close to UEs but may be incapable of big data processing. The latest white paper published by ETSI has further illustrated that central cloud computing and edge computing are highly complementary and significant benefits can be attained when utilizing both [3]. Therefore, this paper studies the deployment of heterogeneous edge and central clouds to enhance cloud computing in future wireless networks. To our best knowledge, this is the first work addressing the integrated edge and central cloud computing in heterogeneous cellular networks (HetNets) with wireless backhaul.

Our main contributions are summarized as follows:

- **Hybrid Edge/Central Cloud Computing Architecture:** we consider a hybrid edge and central cloud computing architecture in a two-tier HetNet, where UEs can offload their computing tasks to the SBSs with limited edge computing capabilities, or to macro BS (MBS) provides central cloud computing services via multiple-input multiple-output (MIMO)/massive MIMO backhaul.
- **Problem Formulation for Joint Cloud Selection, Access Transmit Power, Receive Beamforming and Backhaul Transmit Covariance Matrix Optimization:** Our aim is to minimize the network's energy consumption under edge computing and backhaul latency constraint through jointly optimizing the cloud selection, the UE's transmit power, the SBS's receive beamforming vector, and the SBS's transmit covariance matrix. Moreover, the edge computing latency should not exceed the targeted values, and the computing process of central cloud shall be faster than that of edge cloud. A mixed-integer and non-convex optimization problem is formulated accordingly. For the case of massive MIMO backhaul, we consider two low-complexity linear processing methods, namely maximal-ratio combining (MRC) and zero-forcing (ZF).
- **Algorithm Design:** An iterative algorithm is developed to solve such combinatorial problem. In particular, we show that in each iteration, UE's transmit power and SBS's receive beamforming vector can be optimized in closed-form, and SBS's transmit covariance matrix solution is obtained by leveraging a successive pseudoconvex optimization approach. In addition, low-complexity massive MIMO backhaul solutions can be easily obtained thanks to the unique features of massive MIMO transmission.
- **Design Insights:** Simulation results are presented to demonstrate the efficiency of the proposed algorithm and shed light on the effects of key parameters such as edge cloud's CPU frequency and offloaded task size. The proposed solution outperforms the conventional

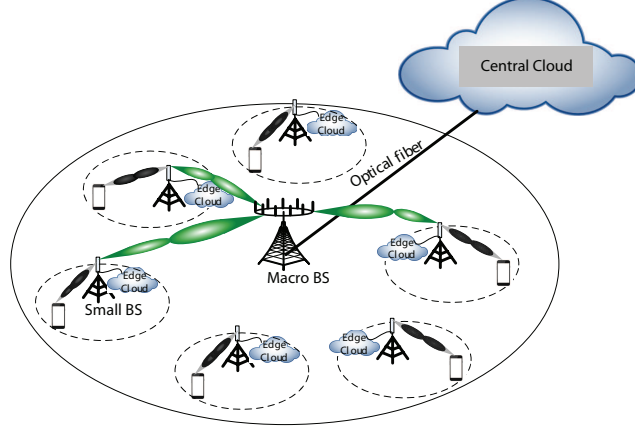


Fig. 1. An illustration of two-tier HetNets powered by traditional cloud computing (central) and edge computing, where MIMO/massive MIMO backhaul provides central cloud computing for addressing more complicated computing tasks which cannot be handled by edge cloud due to limited computing ability.

ones. It is confirmed that the integrated edge and central cloud computing proposed in this work can achieve better performance than edge-only cloud computing or central-only cloud computing. In addition, low-complexity massive MIMO solutions could outperform the traditional MIMO ones in certain scenarios.

The rest of this paper is organized as follows. In Section II, the considered system model is described and the corresponding optimization problem is formulated. The proposed algorithm under traditional MIMO backhaul is presented in Section III, and massive MIMO backhaul solution is given in Section IV. Section V provides the simulation results. Finally, we have some concluding remarks in Section VI.

Notations—In this paper, the notations $(\cdot)^H$ and $(\cdot)^\dagger$ are conjugate transpose and conjugate operators, respectively. In addition, $[x]^+ \triangleq \max\{x, 0\}$, $\det(\mathbf{A})$ denotes the determinant of \mathbf{A} , and $\text{tr}\{\mathbf{A}\}$ is the trace of \mathbf{A} . Also, $\text{eig}\{\mathbf{A}\}$ denotes the set of all the eigenvalues for \mathbf{A} , and $\text{eigvec}\{\cdot\}$ gives the eigenvector for a given eigenvalue of \mathbf{A} and $\langle \mathbf{A}_1, \mathbf{A}_2 \rangle \triangleq \Re\{\text{tr}(\mathbf{A}_1^H \mathbf{A}_2)\}$, where $\Re\{\cdot\}$ is the real-value operator.

II. SYSTEM MODEL AND PROBLEM FORMULATION

As shown in Fig. 1, we consider a two-tier HetNet, where an M -antenna MBS provides high-speed wireless backhaul and is fiber-optic connected to the central cloud with super computing capability, and N SBSs with edge clouds can provide limited computing capabilities. In each

small cell, a SBS equipped with L antennas serves a single-antenna UE, and each UE has an atomic computation-intensive task which cannot be divided and has to be offloaded for computation. The case of serving multiple UEs in each small cell can be dealt with by using existing orthogonal multiple access techniques such as time/frequency-division. Let $\mathcal{N} = \{1, \dots, N\}$ denote the set of the SBSs and UEs, and $B^a = (1 - \rho)B$ and $B^b = \rho B$ ($\rho \in (0, 1)$) denote the bandwidths allocated to the access and backhaul links, respectively, where B is the system bandwidth.

Since the computing tasks offloaded by the UEs could be executed either at the edge cloud or central cloud, cloud selection needs to be appropriately determined before evaluating the computation latency and energy consumption. Let the binary indicator c_n denote the computing decision, where $c_n = 1$ indicates edge computing, and $c_n = 0$ indicates central cloud computing for each UE $n \in \mathcal{N}$. In the sequel, we will study the latency and energy consumption of the network, and then formulate the optimization problem for minimizing the network's total energy consumption under the delay constraints.

A. Transmission and Computing Latency

1) *Access Transmission Latency*: The uplink transmission rate for offloading the computing tasks of UE n to its serving SBS is

$$R_n^a(\mathbf{p}^u, \mathbf{w}_n) = B^a \log_2 (1 + \gamma_n^a(\mathbf{p}^u, \mathbf{w}_n)) \quad (1)$$

with the signal-to-interference-plus-noise ratio (SINR)

$$\gamma_n^a(\mathbf{p}^u, \mathbf{w}_n) = \frac{p_n^u |\mathbf{w}_n^H \mathbf{h}_{n,n}^a|^2}{\sum_{i=1, i \neq n}^N p_i^u |\mathbf{w}_n^H \mathbf{h}_{i,n}^a|^2 + |\mathbf{w}_n^H \mathbf{n}_n|^2}, \quad (2)$$

where \mathbf{w}_n is the receive beamforming vector of the n -th SBS, $\mathbf{h}_{i,n}^a \in \mathbb{C}^{L \times 1}$ is the channel vector between UE i and SBS n , \mathbf{n}_n is a vector of additive white Gaussian noise with zero mean and variance σ_n^2 , and $\mathbf{p}^u \triangleq [p_1^u, \dots, p_N^u]^T \in \mathbb{R}^{N \times 1}$ denotes the transmit power vector of the UEs. Therefore, given an arbitrary offloaded computation task size of the n -th UE's, denoted as I_n (bits), its uplink transmission latency for task offloading is calculated as

$$T_n^a(\mathbf{p}^u, \mathbf{w}_n) = \frac{I_n}{R_n^a(\mathbf{p}^u, \mathbf{w}_n)}. \quad (3)$$

2) *Edge Computing Latency* ($c_n = 1$): Let f and ϑ denote the SBS's CPU clock frequency and the number of CPU cycles per bit data required for edge computing, respectively. The computation latency at the n -th SBS can be described as

$$T_n^{\text{edge}} = \frac{\vartheta I_n}{f}, \quad (4)$$

which indicates that the amount of edge computing latency heavily depends on the offloaded task size and edge cloud's CPU clock frequency.

3) *Central Cloud Processing Latency* ($c_n = 0$): The central cloud processing latency results from backhaul transmission and task execution at the central cloud. Due to the central cloud's super computing capability, its computing time is much lower than edge computing, thus we assume that the central cloud computing time is negligible. Hence, the central cloud processing latency, i.e., the backhaul transmission delay for the n -th UE is calculated as transmission rate given by

$$T_n^{\text{central}}(\mathbf{Q}) = \frac{I_n}{R_n^{\text{b}}(\mathbf{Q})}, \quad (5)$$

where $R_n^{\text{b}}(\mathbf{Q})$ is the backhaul transmission rate given by

$$R_n^{\text{b}}(\mathbf{Q}) = B^{\text{b}} \log_2 \det \left(\mathbf{I} + \Psi(\mathbf{Q}_{-n})^{-1} \mathbf{H}_n^{\text{b}} \mathbf{Q}_n (\mathbf{H}_n^{\text{b}})^H \right), \quad (6)$$

with the noise-plus-interference covariance matrix denoted as $\Psi(\mathbf{Q}_{-n}) = \sigma^2 \mathbf{I} + \sum_{i=1, i \neq n}^N \mathbf{H}_i^{\text{b}} \mathbf{Q}_i (\mathbf{H}_i^{\text{b}})^H$. In (6), \mathbf{Q}_n is the transmit covariance matrix of SBS n , $\mathbf{Q} = \{\mathbf{Q}_n\}_{n=1}^N$ and $\mathbf{Q}_{-n} = \{\mathbf{Q}_i\}_{i=1, i \neq n}^N$ are the compact transmit covariance matrices and the compact transmit covariance matrices except \mathbf{Q}_n , respectively, and $\mathbf{H}_n^{\text{b}} \in \mathbb{C}^{M \times L}$ is the backhaul channel matrix from SBS n to the MBS. Note that if the task of UE i is executed by the edge cloud of SBS i , i.e. $c_i = 1$, the transmit covariance matrix at SBS i will be $\mathbf{Q}_i = \mathbf{0}$.

In addition, it is assumed that the size of computing outputs (usually a few command bits) is small and the downlink overhead such as time and energy consumption for delivering them to the UEs is negligible and therefore ignored.

B. Energy Consumption

Energy consumption results from task offloading energy and task execution energy. Based on Section II-A, the amount of energy consumption for UE n to offload its computing tasks to its serving SBS is

$$E_n^{\text{a}} = p_n^{\text{u}} T_n^{\text{a}}(\mathbf{p}^{\text{u}}, \mathbf{w}_n). \quad (7)$$

If the task is executed by the edge cloud at the SBS, the energy consumption is given by

$$E_n^{\text{edge}} = \varrho I_n \vartheta f^2, \quad (8)$$

where ϱ is the effective switched capacitance of the edge server. Else, if the task is executed by the central cloud, we then have

$$E_n^{\text{central}} = \text{tr}(\mathbf{Q}_n) T_n^{\text{central}}(\mathbf{Q}) + \zeta E_n^{\text{edge}}, \quad (9)$$

where ζ is the ratio of central cloud's energy consumption to that of the edge cloud for computing the same task. Thus, the total energy consumption can be calculated as¹

$$E_{\text{total}} = \sum_{n=1}^N (E_n^{\text{a}} + c_n E_n^{\text{edge}} + (1 - c_n) E_n^{\text{central}}). \quad (10)$$

C. Problem Formulation

Our aim is to minimize the total energy consumption under computation latency constraints through jointly optimizing the UEs' transmit power, the receive beamformers at the SBSs, and the SBSs' transmit covariance matrix. To this end, the problem is formulated as

$$\begin{aligned} \min_{\mathbf{c}, \mathbf{p}^{\text{u}}, \mathbf{w}, \mathbf{Q}} \quad & E_{\text{total}} \\ \text{s.t.} \quad & \text{C1 : } c_n \in \{0, 1\}, \quad \forall n \in \mathcal{N}, \\ & \text{C2 : } T_n^{\text{a}}(\mathbf{p}^{\text{u}}, \mathbf{w}_n) + c_n T_n^{\text{edge}} \leq T_{\text{th}}, \quad \forall n \in \mathcal{N}, \\ & \text{C3 : } (1 - c_n) T_n^{\text{central}}(\mathbf{Q}) \leq \alpha T_n^{\text{edge}}, \quad \forall n \in \mathcal{N}, \\ & \text{C4 : } 0 \leq p_n^{\text{u}} \leq P_{\text{max}}^{\text{u}}, \quad \forall n \in \mathcal{N}, \\ & \text{C5 : } \mathbf{Q}_n \succeq \mathbf{0}, \quad \forall n \in \mathcal{N}, \end{aligned} \quad (11)$$

where $\mathbf{c} = \{c_n\}_{n=1}^N$ and $\mathbf{w} = \{\mathbf{w}_n\}_{n=1}^N$. Constraint C2 is the latency constraint of edge processing, such that the sum of the access transmission latency and the edge computing latency should not exceed a threshold T_{th} ; As illustrated in subsection II-A2 and II-A3, C3 ensures that central cloud processing latency (backhaul latency) shall be lower than edge computing latency in practice, which means that central cloud will be the only option to be utilized as edge cloud cannot meet its latency constraint in C2, i.e., edge and central cloud computing are complementary [3]. Here,

¹Here, the static energy consumption of UEs and SBSs consumed by the circuit or cooling is ignored since it has negligible effect on our design.

α ($0 \leq \alpha < 1$) is the predefined fraction for a specified scenario. For the special case of $\alpha = 0$, central cloud becomes unavailable as indicated in C3, and problem (11) reduces to resource allocation problem in MEC networks, which has been studied from different perspectives in the literature such as [11–14, 16–21].

III. ALGORITHM DESIGN

The considered problem (11) is a mixed-integer and non-convex optimization problem, which is NP-hard in general. To be tractable, we first need to determine whether edge or central cloud computing will be employed, and then we can optimize the transmit power, beamformer and covariance matrix. Hence, a tractable approach can be developed to solve (11) in an iterative manner given below.

A. Edge or Central Cloud Computing

When the n -th SBS's edge computing time T_n^{edge} is greater than the maximum allowable time T_{th} , the use of edge cloud is infeasible and central cloud computing has to be utilized, i.e., $c_n = 0$. When $T_n^{\text{edge}} < T_{\text{th}}$, we adopt the decomposition approach, considering the fact that \mathbf{c} and $\{\mathbf{p}^u, \mathbf{w}, \mathbf{Q}\}$ are coupled in the objective function and constraint C2 of problem (11). By relaxing $c_n \in \{0, 1\}$ to $c_n \in [0, 1]$, we find that given $\{\mathbf{p}^u, \mathbf{w}, \mathbf{Q}\}$, problem (11) can be decomposed into

$$\begin{aligned} \min_{\mathbf{c}} \quad & \sum_{n=1}^N (c_n E_n^{\text{edge}} + (1 - c_n) E_n^{\text{central}}) \\ \text{s.t.} \quad & \text{C1 : } c_n \in [0, 1], \quad \text{C2,} \quad \text{C3.} \end{aligned} \quad (12)$$

Problem (12) is a one-dimensional linear programming, and its solution can be given in two cases:

- Case 1: Without loss of generality, if the energy consumption of edge computing is lower than that of central cloud computing at the UE n , i.e., $E_n^{\text{edge}} \leq E_n^{\text{central}}$, the objective function in (12) is a decreasing function of c_n . Therefore, the optimal c_n^* is the maximum value that satisfies C1-C3, i.e.,

$$c_n^* = \left[\min \left\{ \frac{T_{\text{th}} - T_n^a(\mathbf{p}^u, \mathbf{w}_n)}{T_n^{\text{edge}}}, 1 \right\} \right]^+. \quad (13)$$

- Case 2: if $E_n^{\text{edge}} > E_n^{\text{central}}$, the objective function in (12) is an increasing function of c_n , and the optimal c_n^* is the minimum value that satisfies C1-C3, i.e.,

$$c_n^* = \left[1 - \frac{\alpha T_n^{\text{edge}}}{T_n^{\text{central}}(\mathbf{Q})} \right]^+. \quad (14)$$

It is seen that the edge/central cloud computing decision \mathbf{c}^* is reliant on the optimal $\{\mathbf{p}^u, \mathbf{w}, \mathbf{Q}\}$ of problem (11). In the following two subsections, we will focus on obtaining the optimal $\{\mathbf{p}^{u*}, \mathbf{w}^*\}$ and \mathbf{Q}^* , respectively, based on a given cloud selection decision \mathbf{c} .

B. UE's Transmit Power and SBS's Receive Beamformer

For fixed cloud selection \mathbf{c} , the optimal $\{\mathbf{p}^{u*}, \mathbf{w}^*\}$ can be obtained by solving the subproblem of (11) as follows:

$$\begin{aligned} \min_{\mathbf{p}^u, \mathbf{w}} \quad & \sum_{n=1}^N p_n^u T_n^a(\mathbf{p}^u, \mathbf{w}_n) \\ \text{s.t.} \quad & \text{C2, C4.} \end{aligned} \quad (15)$$

The subproblem (15) is non-convex (over \mathbf{p}^u) and its objective function is the weighted sum-of-ratios, which is challenging to solve. We first examine the interplay between the UEs' transmit power \mathbf{p}^u and the SBS's receive beamformer \mathbf{w} .

Lemma 1. *For fixed \mathbf{p}^u , the optimal \mathbf{w}_n^* of problem (15) is given by*

$$\mathbf{w}_n^* = \text{eigvec} \left\{ \max \left\{ \text{eig} \left\{ (\boldsymbol{\Omega}_{-n})^{-1} \boldsymbol{\Omega}_n \right\} \right\} \right\}, \quad (16)$$

where $\boldsymbol{\Omega}_{-n} = \sigma_n^2 \mathbf{I}_L + \sum_{i=1, i \neq n}^N p_i^u \mathbf{h}_{i,n}^a (\mathbf{h}_{i,n}^a)^H$ and $\boldsymbol{\Omega}_n = p_n^u \mathbf{h}_{n,n}^a (\mathbf{h}_{n,n}^a)^H$.

Proof. See Appendix A. □

With the help of auxiliary variables $\mathbf{t} = \{t_n\}_{n=1}^N$, problem (15) over the UEs' transmit power vector \mathbf{p}^u for fixed \mathbf{w} can be equivalently transformed as

$$\begin{aligned} \min_{\mathbf{p}^u, \mathbf{t}} \quad & \sum_{n=1}^N I_n t_n \\ \text{s.t.} \quad & \tilde{\text{C1}} : \frac{p_n^u}{R_n^a(\mathbf{p}^u, \mathbf{w}_n)} \leq t_n, \quad \forall n \in \mathcal{N}, \\ & \tilde{\text{C2}} : \gamma_n^a(\mathbf{p}^u, \mathbf{w}_n) \geq \tau, \quad \forall n \in \mathcal{N} \\ & \tilde{\text{C3}} : 0 \leq p_n^u \leq P_{\max}^u, \quad \forall n \in \mathcal{N} \end{aligned} \quad (17)$$

where $\tau = 2^{\frac{I_n}{B^a(T_{\text{th}} - c_n T_n^{\text{edge}})}} - 1$.

Lemma 2. *The optimal solution $(\mathbf{p}^{\text{u}*}, \mathbf{t}^*)$ of problem (17) satisfies the Karush-Kuhn-Tucker (KKT) conditions of the following N ($n \in \mathcal{N}$) subproblems*

$$\begin{aligned} \min_{p_n^{\text{u}}} \quad & (\lambda_n + M_n) p_n^{\text{u}} - \lambda_n t_n R_n^{\text{a}}(\mathbf{p}^{\text{u}}, \mathbf{w}_n) \\ \text{s.t.} \quad & \tilde{\text{C2}} : \gamma_n^{\text{a}}(\mathbf{p}^{\text{u}}, \mathbf{w}_n) \geq \tau, \\ & \tilde{\text{C3}} : 0 \leq p_n^{\text{u}} \leq P_{\max}^{\text{u}}, \end{aligned} \quad (18)$$

with

$$\begin{aligned} M_n = \sum_{j=1, j \neq n}^N \lambda_j t_j \frac{B_{\text{a}}}{\ln 2} \frac{(\gamma_j^{\text{a}})^2 |\mathbf{w}_j^H \mathbf{h}_{n,j}^{\text{a}}|^2}{p_j^{\text{u}} |\mathbf{w}_j^H \mathbf{h}_{j,j}^{\text{a}}|^2 (1 + \gamma_j^{\text{a}})} + \\ \sum_{j=1, j \neq n}^N \mu_j \frac{(\gamma_j^{\text{a}})^2 |\mathbf{w}_j^H \mathbf{h}_{n,j}^{\text{a}}|^2}{p_j^{\text{u}} |\mathbf{w}_j^H \mathbf{h}_{j,j}^{\text{a}}|^2}, \end{aligned} \quad (19)$$

where $\{\lambda_n\}_{n=1}^N$ and $\{\mu_j\}_{n=1}^N$ are Lagrange multipliers associated with the constraints $\tilde{\text{C1}}$ and $\tilde{\text{C2}}$ of problem (17), respectively. For optimal $(\mathbf{p}^{\text{u}*}, \mathbf{t}^*)$, λ_n and t_n are respectively calculated as

$$\lambda_n = \frac{I_n}{R_n^{\text{a}}(\mathbf{p}^{\text{u}*}, \mathbf{w}_n^*)}, \quad (20)$$

$$t_n = \frac{p_n^{\text{u}*}}{R_n^{\text{a}}(\mathbf{p}^{\text{u}*}, \mathbf{w}_n^*)}. \quad (21)$$

Proof. See Appendix B. □

Given λ_n and t_n , subproblem (18) is convex with respect to (w.r.t.) p_n^{u} . Therefore, we have the following theorem.

Theorem 1. *The solution of subproblem (18) is given by*

$$p_n^{\text{u}*} = \begin{cases} \frac{\tau}{\Lambda_n}, & \text{if } G_n < \frac{\tau}{\Lambda_n}, \\ G_n, & \text{if } \frac{\tau}{\Lambda_n} \leq G_n \leq P_{\max}^{\text{u}}, \\ P_{\max}^{\text{u}}, & \text{if } G_n > P_{\max}^{\text{u}}, \end{cases} \quad (22)$$

$$\mu_n^* = \begin{cases} \frac{\lambda_n + M_n}{\Lambda_n} - \frac{B_{\text{a}}}{\ln 2} \frac{\lambda_n t_n}{\tau + 1}, & \text{if } G_n < \frac{\tau}{\Lambda_n}, \\ 0, & \text{otherwise,} \end{cases} \quad (23)$$

$$\nu_n^* = \begin{cases} 0, & \text{if } G_n \leq P_{\max}^{\text{u}}, \\ \frac{B_{\text{a}}}{\ln 2} \frac{\lambda_n t_n}{P_{\max}^{\text{u}} + 1/\Lambda_n} - \lambda_n - M_n, & \text{otherwise,} \end{cases} \quad (24)$$

where we define $\Lambda_n \triangleq \frac{|\mathbf{w}_n^H \mathbf{h}_{n,n}^a|^2}{\sum_{i=1, i \neq n}^N p_i^u |\mathbf{w}_n^H \mathbf{h}_{i,n}^a|^2 + |\mathbf{w}_n^H \mathbf{n}_n|^2}$, $G_n \triangleq \frac{B_a}{\ln 2} \frac{\lambda_n t_n}{\lambda_n + M_n} - \frac{1}{\Lambda_n}$, and μ_n^* and ν_n^* are respectively the optimal Lagrange multipliers associated with the constraints $\tilde{\text{C2}}$ and $\tilde{\text{C3}}$ of problem (18).

Proof. See Appendix C. □

In light of the results in **Lemma 1**, **Lemma 2** and **Theorem 1**, we provide an iterative approach to solve problem (15), which is shown in **Algorithm 1**.

Algorithm 1 Solution of Problem (15)

- 1: **Initialize** $p_n^u = P_{\max}^u$, $\forall n$. Set \mathbf{w}_n based on **Lemma 1**.
 - 2: **Repeat**
 - 3: a) Given \mathbf{w} , Loop:
 - i): Compute M_n , λ_n and t_n based on **Lemma 2**.
 - ii): Update p_n^u and μ_n based on **Theorem 1**.
 Until convergence.
 - 4: b) Update \mathbf{w} based on **Lemma 1**.
 - 5: Until convergence, and obtain optimal $\{\mathbf{p}^{u*}, \mathbf{w}^*\}$.
-

The convergence of **Algorithm 1** can be guaranteed since the objective function of problem (15) decreases with the iteration index (in step 3 and step 4 of **Algorithm 1**), which is indicated from optimizing \mathbf{p}^u and \mathbf{w} in each iteration as shown in **Lemma 1** and **Lemma 2**, respectively.

C. SBS's Transmit Covariance Matrix

For fixed cloud selection \mathbf{c} , the optimal \mathbf{Q}^* can be obtained by solving the following sub-problem:

$$\begin{aligned}
 \min_{\mathbf{Q}} \quad & y(\mathbf{Q}) = \sum_{n=1}^N (1-c_n) \text{tr}(\mathbf{Q}_n) T_n^{\text{central}}(\mathbf{Q}) \\
 \text{s.t.} \quad & \text{C3} : R_n^b(\mathbf{Q}) \geq (1-c_n) \frac{I_n}{\alpha T_n^{\text{edge}}}, \quad \forall n \in \mathcal{N}, \quad \text{C5}.
 \end{aligned} \tag{25}$$

Problem (25) is non-convex due to the non-convexity of the objective function and constraint C3, which cannot be solved directly. Thus, we resort to a successive pseudoconvex approach to solve it, which has many advantages such as fast convergence and parallel computation [22].

First, let \mathbf{Q}^l denote the \mathbf{Q} value in the l -th iteration. Thus non-convex $\text{tr}(\mathbf{Q}_n) T_n^{\text{central}}(\mathbf{Q})$ in the objective function can be approximated as a pseudoconvex function at \mathbf{Q}^l , which is written as

$$\hat{y}_n(\mathbf{Q}_n; \mathbf{Q}^l) \triangleq \frac{I_n \text{tr}(\mathbf{Q}_n)}{R_n^b(\mathbf{Q}_n; \mathbf{Q}^l)} + z_n(\mathbf{Q}_n), \quad (26)$$

where $z_n(\mathbf{Q}_n) = \sum_{j \neq n} I_j \text{tr}(\mathbf{Q}_j^l) \left\langle (\mathbf{Q}_n - \mathbf{Q}_n^l), \nabla_{\mathbf{Q}_n^l} \frac{1-c_j}{R_j^b(\mathbf{Q}^l)} \right\rangle$ is a function obtained by linearizing the non-convex function $\sum_{j \neq n} \text{tr}(\mathbf{Q}_j) T_j^{\text{central}}(\mathbf{Q})$ in \mathbf{Q}_n at the point \mathbf{Q}^l and $\nabla_{\mathbf{Q}_j^l} \frac{1-c_j}{R_j^b(\mathbf{Q}^l)}$ is the Jacobian matrix of $\frac{1-c_j}{R_j^b(\mathbf{Q}^l)}$ w.r.t. \mathbf{Q}_j^l . Based on (26), we can approximate the objective function $y(\mathbf{Q})$ of problem (25) at \mathbf{Q}^l as

$$\tilde{y}(\mathbf{Q}; \mathbf{Q}^l) = \sum_{n=1}^N (1-c_n) \hat{y}_n(\mathbf{Q}_n; \mathbf{Q}^l). \quad (27)$$

It is easily seen that $\tilde{y}(\mathbf{Q}; \mathbf{Q}^l)$ is pseudoconvex and has the same gradient with $y(\mathbf{Q})$ at $\mathbf{Q} = \mathbf{Q}^l$.

Then, by leveraging the first-order Taylor expansion at \mathbf{Q}^l , the left-hand-side of the non-convex constraint C3 can be approximated as

$$\begin{aligned} R_n^b(\mathbf{Q}) &= B^b \log_2 \det(\sigma^2 \mathbf{I} + \Xi(\mathbf{Q})) - R_n^{\text{b}2}(\mathbf{Q}) \\ &\approx B^b \log_2 \det(\sigma^2 \mathbf{I} + \Xi(\mathbf{Q})) - R_n^{\text{b}2}(\mathbf{Q}^l) - \\ &\quad \sum_{j \neq n}^N \left\langle (\mathbf{Q}_j - \mathbf{Q}_j^l), \nabla_{\mathbf{Q}_j^l} R_n^{\text{b}2}(\mathbf{Q}^l) \right\rangle \triangleq \bar{R}_n^b(\mathbf{Q}), \end{aligned} \quad (28)$$

where $\Xi(\mathbf{Q}) = \sum_{i=1}^N \mathbf{H}_i^b \mathbf{Q}_i (\mathbf{H}_i^b)^H$, and $R_n^{\text{b}2}(\mathbf{Q}) = B^b \log_2 \det(\sigma^2 \mathbf{I} + \sum_{i \neq n}^N \mathbf{H}_i^b \mathbf{Q}_i (\mathbf{H}_i^b)^H)$. Here, $\bar{R}_n^b(\mathbf{Q})$ is a concave function over \mathbf{Q} .

Therefore, at \mathbf{Q}^l , the original problem (25) can be approximately transformed as

$$\begin{aligned} \min_{\mathbf{Q}} \quad & \tilde{y}(\mathbf{Q}; \mathbf{Q}^l) \\ \text{s.t.} \quad & \bar{R}_n^b(\mathbf{Q}) \geq (1-c_n) \frac{I_n}{\alpha T_n^{\text{edge}}}, \quad \forall n \in \mathcal{N}, \quad \text{C5.} \end{aligned} \quad (29)$$

The objective function of problem (29) is a sum of N pseudoconvex functions including fractional functions and linear functions. In addition, all the constraints in problem (29) are convex. Hence, by leveraging the Dinkelbach-like algorithm [23] and introducing a set of auxiliary variables for the N fractional functions in the objective function, problem (29) can be transformed into a solvable convex optimization problem, which owns provable convergence [22]. Let $\mathbb{B}\mathbf{Q}^l$ represent

the solution of problem (29) at the l -th iteration, and thus the value of \mathbf{Q} in the next $(l + 1)$ -th iteration can be updated as

$$\mathbf{Q}^{l+1} = \mathbf{Q}^l + \varsigma(l)(\mathbb{B}\mathbf{Q}^l - \mathbf{Q}^l), \quad (30)$$

where $\varsigma(l)$ is the step size at the l -th iteration and can be obtained through the successive line search, and $\mathbb{B}\mathbf{Q}^l - \mathbf{Q}^l$ is the descent direction of $y(\mathbf{Q})$. Thus, the solution of problem (25) can be iteratively obtained.

Based on the aforementioned analysis of optimizing $\{\mathbf{p}^{u*}, \mathbf{w}^*, \mathbf{Q}^*\}$, **Algorithm 2** is proposed to solve the original problem (11).

Algorithm 2 Solution of Problem (11)

1: **Initialize** $p_n^u = P_{\max}^u, \forall n$. Set \mathbf{w}_n based on **Lemma 1**.

Based on constraint C2 of problem (11), set $c_n = \left[\min \left\{ \frac{T_{\text{th}} - T_n^a(\mathbf{p}^u, \mathbf{w}_n)}{T_n^{\text{edge}}}, 1 - \delta \right\} \right]^+$, where $\delta \in (0, 0.5)$ is the tolerant value to avoid solely edge cloud or central cloud at the initial point. Then, based on constraint C3 of problem (11), \mathbf{Q} is set to meet $T_n^{\text{central}}(\mathbf{Q}) = \frac{\alpha T_n^{\text{edge}}}{1 - c_n}$ through the use of ZF precoding with equal power allocation at each SBS.

2: **Repeat**

3: a) Given $\{c_n\}_{n=1}^N$:

i): Update $\{\mathbf{p}^u, \mathbf{w}\}$ based on **Algorithm 1**.

ii): Loop:

ii-1): Solve problem (29) via Dinkelbach-like algorithm [23].

ii-2): Update \mathbf{Q}^l based on (30).

Until convergence, and obtain the updated \mathbf{Q} .

4: b) Update $\{c_n\}_{n=1}^N$ according to subsection III-A.

5: Until convergence, and obtain optimal $\{\mathbf{c}^*, \mathbf{p}^{u*}, \mathbf{w}^*, \mathbf{Q}^*\}$,

in which \mathbf{c}^* is obtained by rounding the cloud selection solution of problem (12).

D. Convergence and Complexity

The convergence of **Algorithm 2** is easy to prove in light of the guaranteed convergency of **Algorithm 1**, the Dinkelbach-like algorithm used to solve problem (29), and the update

process of the cloud selection \mathbf{c} illustrated in Section III-A. Note that the objective function of problem (12) is a decreasing function of the iteration index (in step 3 and step 4 of **Algorithm 2**), which ensures the convergence of **Algorithm 2**.

The proposed **Algorithm 2** enjoys an acceptable complexity as well as an easy implementation. In each iteration, the majority of computational complexity lies in solving subproblem (15) for obtaining optimal $(\mathbf{p}^{u*}, \mathbf{w}^*)$ and the approximate subproblem (29) for obtaining optimal \mathbf{Q}^* . In the proposed algorithm, problem (15) can be equivalently transformed into N independent subproblems (17) and thus can be easily solved in a parallel way. Moreover, the optimal solution of each subproblem has closed-form expression as indicated in **Lemma 1**, which only generates a complexity ordered by $\mathcal{O}(N)$. For the approximate subproblem (29), the Dinkelbach-like algorithm is proved to exhibit a linear convergence rate [23] and the corresponding convex optimization problem can be efficiently solved by CVX, thus the generated complexity is acceptable in general. In order to further reduce the complexity of solving the optimization problem for energy saving, we will consider the case of applying the massive MIMO technology at the MBS in the following section, which demonstrates that the complexity of the proposed algorithm can be substantially reduced and better performance are achieved compared to existing schemes.

IV. MASSIVE MIMO BACKHAUL

In the prior section, we have studied the combination of edge-central cloud computing with traditional multi-cell MIMO backhaul. Since massive MIMO has been one of key 5G radio-access technologies, in this section, we further consider the time-division duplex (TDD) massive MIMO aided backhaul in the Rayleigh fading environment, i.e., MBS is equipped with a very large number of antennas and SBS only uses one single transmit antenna ($M \gg N$).

There are two main merits for massive MIMO backhaul transmission: 1) Since SBSs and MBSs are usually still and the backhaul channels will become deterministic, a phenomenon known as “channel hardening” [24, 25], and thus the backhaul channel coherence time will be much longer than ever before, which means that the time spent on uplink channel estimation will be much lower. Some real-time massive MIMO channel measurement works such as [26] also demonstrated that the use of massive antennas can mitigate the fast-fade error bursts, and enable much less frequent update of power control in low-mobility environments compared to the single-antenna case (see [26, Fig. 8]); 2) As shown in [27], simple linear processing methods can

achieve nearly-optimal performance. As a result, we will consider two linear detection schemes at the MBS, namely MRC and ZF, to provide low-complexity massive MIMO backhaul solutions.

A. MRC Receiver at the MBS

When MRC receiver is applied at the MBS, we consider a lower-bound achievable backhaul rate for tractability, which can well approximate the exact massive MIMO transmission rate as confirmed in [28]. As such, given $(\mathbf{c}, \mathbf{p}^u, \mathbf{w})$, the original problem (25) reduces to

$$\begin{aligned} \min_{\mathbf{q}} \quad & \sum_{n=1}^N (1-c_n) q_n \frac{I_n}{R_n^b(\mathbf{q})} \\ \text{s.t.} \quad & \text{C3} : R_n^b(\mathbf{q}) \geq (1-c_n) \frac{I_n}{\alpha T_n^{\text{edge}}}, \forall n, \\ & \text{C5} : q_n \geq 0, \forall n, \end{aligned} \quad (31)$$

where q_n is the n -th SBS's transmit power, $\mathbf{q} = [q_1, \dots, q_N]$, and

$$R_n^b(\mathbf{q}) = B^b \log_2 \left(1 + (M-1) \frac{q_n \beta_n}{\sum_{i \neq n}^N q_i \beta_i + \sigma_n^2} \right), \quad (32)$$

in which β_i is the large-scale fading coefficient of the link between SBS i and the MBS [28]. Problem (31) is non-convex, but can be equivalent to problem (15) with $\mathbf{w}_n = 1$. Thus, it can be directly solved by using **Algorithm 1**. Note that when using **Algorithm 1**, the initial feasible $\mathbf{q} = [q_1, \dots, q_N]$ needs to be carefully selected. Here, we assume that present fractional power control solution applied in 3GPP-LTE [29] can satisfy the constraint C3, i.e., $q_n = (d_n)^{\epsilon \varpi^b}$, where d_n is the communication distance between the n -th SBS and the MBS, $\epsilon \in [0, 1]$ is the pathloss compensation factor, and ϖ^b is the pathloss exponent of the backhaul link. For the special case of full compensation ($\epsilon = 1$), the number of MBS's antennas needs to meet

$$M \geq 1 + (N-1) \left(2^{\frac{(1-c_n)I_n}{B^b \alpha T_n^{\text{edge}}}} - 1 \right). \quad (33)$$

B. ZF Receiver at the MBS

When ZF receiver is applied at the MBS, we adopt the corresponding tight lower-bound achievable rate shown in [28]. Given $(\mathbf{c}, \mathbf{p}^u, \mathbf{w})$, the original problem (25) reduces to

$$\begin{aligned} \min_{\mathbf{q}} \quad & \sum_{n=1}^N (1-c_n) \frac{q_n I_n}{R_n^b(q_n)} \\ \text{s.t.} \quad & \text{C3} : R_n^b(q_n) \geq \frac{(1-c_n) I_n}{\alpha T_n^{\text{edge}}}, \forall n \in \mathcal{N}, \end{aligned} \quad (34)$$

$$\text{C5} : q_n \geq 0, \forall n \in \mathcal{N},$$

where

$$R_n^b(q_n) = B^b \log_2 \left(1 + (M - N) \frac{q_n \beta_n}{\sigma_n^2} \right). \quad (35)$$

Since $\frac{q_n}{R_n^b(q_n)}$ is an increasing function of q_n ($\frac{\partial \left(\frac{q_n}{R_n^b(q_n)} \right)}{\partial q_n} \geq 0$), the optimal q_n^* is the minimum value that meets the constraints C3 and C5, i.e.,

$$q_n^* = \frac{2^{\frac{(1-c_n)I_n}{B^b \alpha T_n^{\text{edge}}}} - 1}{(M - N) \frac{\beta_n}{\sigma_n^2}}, \forall n \in \mathcal{N}. \quad (36)$$

Bases on the above analysis, when massive MIMO backhaul is employed at the MBS, the solution of problem (11) can still be obtained by using the proposed **Algorithm 2**, where the optimal SBSs' transmit powers are given by the solution of problem (31) for the MRC receiver or (36) for the ZF receiver.

In comparison with the case of using traditional MIMO backhaul, MRC and ZF linear detection schemes for massive MIMO backhaul links enjoy super-low complexity. For MRC scheme, the problem (31) can be effectively solved by **Algorithm 1**, and its computational complexity is also with the order of $\mathcal{O}(N)$. For ZF scheme, the closed-form solution of problem (34) can be directly obtained, and its complexity order is $\mathcal{O}(1)$.

V. SIMULATION RESULTS

In this section, simulation results are presented to evaluate the performance of the proposed algorithms and shed light on the effects of the key parameters including the ratio of energy consumption between central and edge cloud computing (ζ), the task size (I), the latency threshold of edge processing (T_{th}), the required fraction of edge computing time for backhaul transmission (α), and the SBSs' CPU clock frequency (f). The performance of some practical schemes are also given as benchmarks, including the "Initial feasible solution", "Edge-cloud-only", "Central-cloud-only" schemes, and a scheme with fixed cloud selection, denoted as "Half edge, half central" scheme where half number of UEs choose edge cloud and the other half use central cloud to complete their computing tasks. Note that the performance indicators (total energy consumption and percentage of UEs that select edge cloud computing) shown in the following figures are averaged over 500 independent channel realizations. All the small-scale fading channel coefficients follow independent and identically complex Gaussian distribution

TABLE I
SIMULATION PARAMETERS

Parameter	Symbol	Value
Bandwidth for an access or backhaul link	B^a, B^b	10 MHz
Noise power spectral density for an access or backhaul link	σ_n^2, σ^2	-174 dBm/Hz
Pathloss exponent for access link	ϖ^a	3.67
Pathloss exponent for backhaul link	ϖ^b	2.35
Pathloss compensation factor	ϵ	1
Radius of the small cell	r^a	50 m
Radius of the macro cell	r^b	500 m
Number of SBSs/UEs	N	6
Number of antennas for each SBS	L	2
UEs' maximum transmit power	P_{\max}^u	23 dBm
Required CPU cycles per bit	ϑ	300 cycles/bit
the effective switched capacitance of the SBS processor	ϱ	10^{-28}
The tolerant value in Algorithm 2	δ	0.1

with zero mean and unit variance. The pathloss between SBS and UE and between MBS and SBS are respectively set as $140.7 + 36.7 \log_{10} d(\text{km})$ and $100.7 + 23.5 \log_{10} d(\text{km})$ according to 3GPP TR 36.814 [30], where d is the distance between two nodes. The other basic simulation parameters are listed in Table I.

A. Improvement with Traditional MIMO Backhaul

In this subsection, numerical results for integrated edge and central cloud computing system with traditional MIMO backhaul are presented in comparison with the benchmarks mentioned before, to demonstrate the performance enhancement of using the proposed algorithm through optimizing the key system parameters including cloud selection, UEs' transmit power, SBSs' receive beamformer and transmit covariance matrix.

Fig. 2 shows the effect of different ζ on the total energy consumption of the system. We see that the energy consumption of all the schemes are non-decreasing functions of ζ , due to the fact that the energy cost of central cloud computing increases with ζ . It is confirmed that the proposed solution outperforms all the baselines, which means that energy cost can be significantly reduced. The performance improvement is particularly noticeable compared with the Edge-cloud-only scheme in the range of $\zeta < 1$, the traditional Central-cloud-only scheme

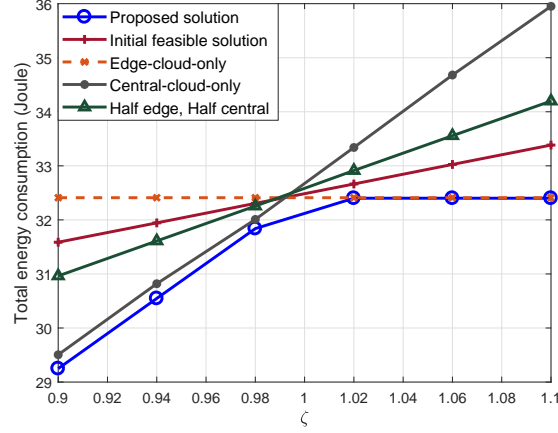


Fig. 2. The total energy consumption of the system with traditional MIMO backhaul versus ζ : $M = 16$, $T_{\text{th}} = 0.3$ s, $\alpha = 0.1$, $I_n = 5$ Mbits.

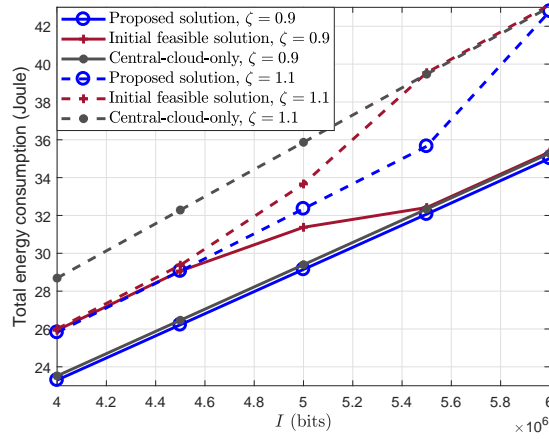


Fig. 3. The total energy consumption of the system with traditional MIMO backhaul versus the task size I : $M = 16$, $T_{\text{th}} = 0.3$ s, $\alpha = 0.1$.

in the range of $\zeta > 1$, and the “Half edge, half central” scheme in the whole range of ζ . In addition, the proposed solution also consumes lower amount of energy than the initial feasible solution.

Fig. 3 shows the total energy consumption of the system versus the task sizes I for the cases of $\zeta = 0.9$ and $\zeta = 1.1$, where $I = I_n$ for $n \in \mathcal{N}$. It is easy to understand that computing more input data consumes more energy, and thus the energy cost of each scheme increases with I . Again, we see that the proposed solution is superior to the baseline solutions in all the cases.

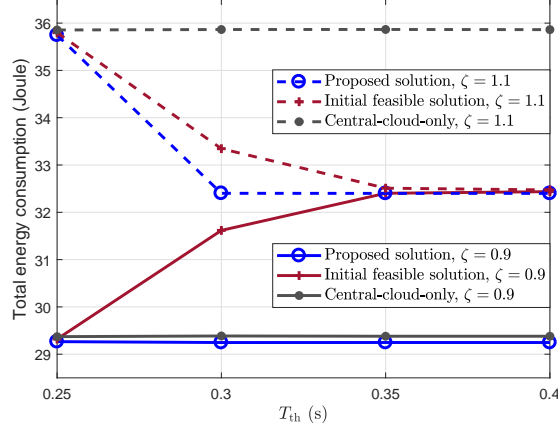


Fig. 4. The total energy consumption of the system with traditional MIMO backhaul versus the latency threshold of edge processing T_{th} : $M = 16$, $I = 5$ Mbits, $\alpha = 0.1$.

For the case of $\zeta = 0.9$, the performance of the Central-cloud-only solution is very close to the proposed one since central cloud is dominant in this case, i.e., more UEs tend to use central cloud computing for saving energy. For the case of $\zeta = 1.1$, the advantage of the proposed scheme becomes more obvious compared with the baselines. We observe that the results of using the proposed solution approach to those of the Central-cloud-only solution when I increases, which means that more UEs will select the central cloud for large task size. The reason is that when the task is large, the edge processing delay constraint **C2** of problem (11) is no longer satisfied due to the limited edge computing capability, and central cloud has to be chosen for computation.

Fig. 4 shows the total energy consumption of the system varying with the latency threshold of edge processing for the cases of $\zeta = 0.9$ and $\zeta = 1.1$. It is seen that the proposed solution is a non-increasing function of T_{th} and outperforms the baselines in both cases. The Central-cloud-only solution is insensitive to T_{th} , and its performance is almost invariant thanks to its super computing capability for low computing latency. Note that all the solutions consume almost same amount of energy when T_{th} is small, e.g., $T_{th} = 0.2$ s in this figure. The reason is that the edge processing latency constraint **C2** cannot met and only central cloud computing can be employed to satisfy the latency constraint. For the case of $\zeta = 0.9$, the performance gap between the proposed solution and the Central-cloud-only is small since central cloud computing is dominant, and both solutions performs better than the Initial feasible solution. It is interesting to note that the Initial feasible solution is an increasing function of $T_{th} \in [0.2, 0.4]$ s when $\zeta = 0.9$, this

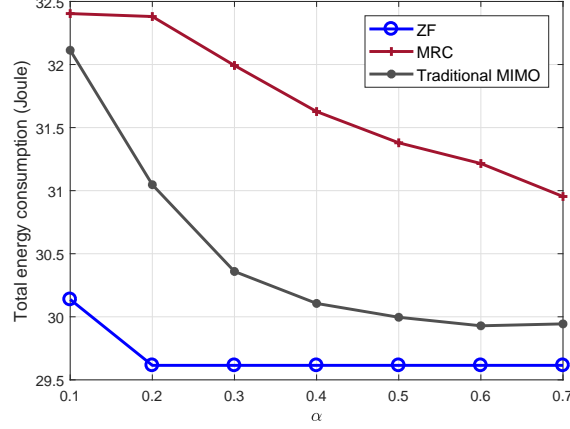


Fig. 5. The total energy consumption of the system versus α : $M = 128$ for massive MIMO backhaul, $M = 8$ for traditional MIMO backhaul, $\zeta = 0.9$, $T_{th} = 0.3$ s, $I = 5$ Mbits.

is because the edge cloud computing becomes more feasible as T_{th} increases, and the initial selection that more UEs choose edge computing result in more energy consumption while in fact central cloud computing saves more energy, which indicates the importance of optimizing cloud selection. For the case of $\zeta = 1.1$, the consumed energy of the proposed solution decreases with T_{th} since more UEs are allowed to choose the energy-efficient edge cloud computing for large T_{th} .

B. Benefits of Massive MIMO Backhaul

In this subsection, we mainly illustrate the performance of the considered edge and central cloud computing system with massive MIMO backhaul, to confirm the benefits of equipping massive antennas at the MBS in improving the system performance. Here, we focus on MRC and ZF beamforming at the MBS, as studied in Section IV.

Fig. 5 and Fig. 6 respectively depict the total energy consumption and the corresponding percentage of UEs that select edge cloud for computing versus α . It is seen from Fig. 5 that the energy consumption of each scheme decreases with α since less power will be used for backhaul transmission as α increases according to the backhaul latency constraint **C3** of problem (11). This result is also reflected by Fig. 6 where the percentage of UEs using edge cloud computing decreases, which means that more UEs choose to use central cloud for computing with increasing α so as to save more energy. Obviously, the energy consumed by the ZF scheme is less than

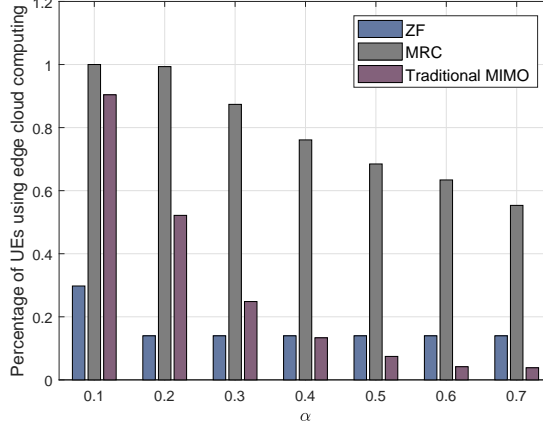


Fig. 6. The percentage of UEs that select edge cloud computing versus α : $M = 128$ for massive MIMO backhaul, $M = 8$ for traditional MIMO backhaul, $\zeta = 0.9$, $T_{th} = 0.3$ s, $I = 5$ Mbits.

that of the MRC scheme and the traditional MIMO backhaul, which demonstrates the benefits of using large antenna arrays at the MBS. Moreover, for the ZF scheme, the percentage of UEs using edge cloud computing is lower than that of the MRC and traditional MIMO schemes when $\alpha < 0.4$. In contrast, the MRC scheme can only use the edge cloud for computing when $\alpha \leq 0.2$. This is because the backhaul latency constraint **C3** in (11) for central cloud processing cannot be satisfied with a small α , when MRC receiver is adopted at the MBS due to the inter-SBS interference. Based on these two figures, we see that the consumed energy of the ZF scheme as well as the corresponding percentage of UEs served by edge cloud decrease very slowly, and is almost unchanged for $\alpha \geq 0.2$, which further indicates that the ZF scheme can provide more stable and higher-speed backhaul transmission for computation tasks offloading.

Fig. 7 shows the total energy consumption of the system versus the task size I for the cases of $\zeta = 0.9$ and $\zeta = 1.1$. Similar to Fig. 3, all the curves increase with I as expected. The ZF scheme outperforms the MRC scheme and the traditional MIMO scheme. For the case of $\zeta = 0.9$, the ZF scheme and the traditional MIMO scheme are dominated by central cloud computing, while the MRC scheme experiences a transition from edge-cloud-dominant to Central-cloud-dominant and more UEs choose to use central cloud for computing so as to satisfy the computing processing latency constraint as well as saving energy. For the case of $\zeta = 1.1$, all the schemes are edge-cloud dominant when $I \leq 5$ Mbits, and then gradually become Central-cloud-dominant as I increases. It is confirmed that the ZF scheme with massive MIMO backhaul has the advantage

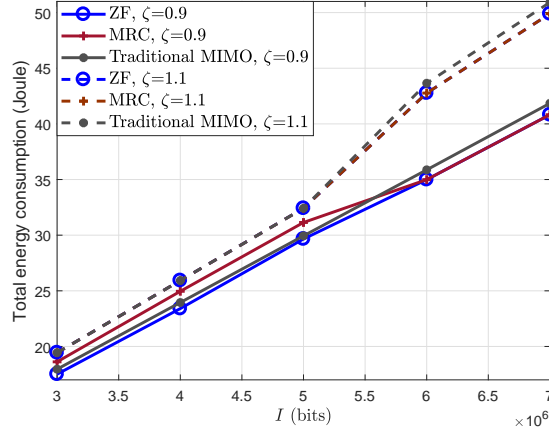
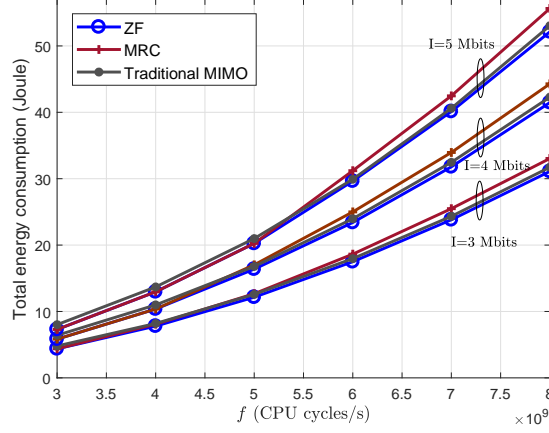


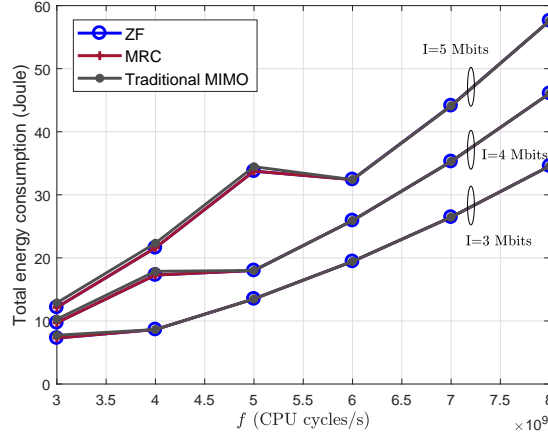
Fig. 7. The total energy consumption of the system versus the task size I : $M = 128$ for massive MIMO backhaul, $M = 8$ for traditional MIMO backhaul, $T_{th} = 0.3$ s, $\alpha = 0.6$.

of handling the computation-intensive tasks.

Fig. 8(a) and Fig. 8(b) show the total energy consumption of the system versus the SBSs' CPU clock frequency (f) in the case of $\zeta = 0.9$ and $\zeta = 1.5$, respectively. According to these two figures, we see that the effect of f is heavily reliant on both the computing task size I and ζ . When I is not large and $\zeta < 1$, network's energy consumption may increase with f as shown in Fig. 8(a), where the curves of all the schemes increase with f and the increasing rates become higher when enlarging I . This is due to the fact that when I is not large and $\zeta < 1$, the energy consumption of the central cloud computing plays a dominant role in contributing to the total energy consumption. In this case, the advantage of using ZF scheme becomes more obvious as f grows large. However, when $\zeta > 1$, network's energy consumption may decrease with f as shown in Fig. 8(b), where there is an obvious decrease as $f \in [5, 6] \times 10^9$ cycles/s in the case of $I = 5$ Mbits. The reason is that when f is small, e.g., less than 4×10^9 cycles/s in Fig. 8(b), the edge processing latency constraint **C2** may be not satisfied and central cloud computing becomes the only option, as f increases, edge cloud computing becomes feasible for more UEs to save energy, and the total energy cost will decrease. In addition, It is seen from Fig. 8(b) that the energy consumption of the three considered schemes are very close since the edge cloud computing is dominant.



(a) $M = 128$ for massive MIMO backhaul, $M = 8$ for traditional MIMO backhaul, $\zeta = 0.9$, $T_{th} = 0.3$ s, $\alpha = 0.6$.



(b) $M = 128$ for massive MIMO backhaul, $M = 8$ for traditional MIMO backhaul, $\zeta = 1.5$, $T_{th} = 0.3$ s, $\alpha = 0.6$.

Fig. 8. The total energy consumption of the system versus SBSs' CPU frequency f .

VI. CONCLUSION

In this paper, we studied the joint design of computing services when edge cloud computing and central cloud computing coexist in a two-tier HetNet with MIMO or massive MIMO self-backhaul. By optimizing the cloud selection, the UE's transmit power, the SBSs' receive beamforming vectors and the transmit covariance matrices, the network's energy consumption can be minimized while meeting both the edge processing and backhaul latency constraints. An iterative algorithm was proposed, which can ensure that the proposed algorithm achieves better performance than any existing feasible solutions. Moreover, we showed that massive

MIMO backhaul can largely decrease the system complexity without loss of the performance. The simulation results have further confirmed by comparing with the existing schemes that the proposed solution can greatly enhance the performance.

APPENDIX A: PROOF OF LEMMA 1

Based on problem (15), we can easily find that each SBS's receive beamformer \mathbf{w}_n aims to maximize the SINR, i.e.,

$$\max_{\mathbf{w}_n} \gamma_n^{(a)}(\mathbf{p}^u, \mathbf{w}_n) \quad (\text{A.1})$$

Problem (A.1) can be rewritten as

$$\max_{\mathbf{w}_n} \frac{\mathbf{w}_n^H \boldsymbol{\Omega}_n \mathbf{w}_n}{\mathbf{w}_n^H \boldsymbol{\Omega}_{-n} \mathbf{w}_n}. \quad (\text{A.2})$$

Note that (A.2) is a generalized eigenvector problem and the optimal \mathbf{w}_n^* is the corresponding eigenvector associated with the largest eigenvalue of the matrix $(\boldsymbol{\Omega}_{-n})^{-1} \boldsymbol{\Omega}_n$. Thus, we obtain the result in (16).

APPENDIX B: PROOF OF LEMMA 2

The lagrange function of problem (17) is

$$\begin{aligned} \mathcal{L}(\mathbf{p}^u, \mathbf{t}, \lambda, \mu, \nu) = & \sum_{n=1}^N I_n t_n + \sum_{n=1}^N \lambda_n (p_n^u - t_n R_n^a(\mathbf{p}^u, \mathbf{w}_n)) \\ & + \sum_{n=1}^N \mu_n (\tau - \gamma_n^a(\mathbf{p}^u, \mathbf{w}_n)) \\ & + \sum_{n=1}^N \nu_n (p_n^u - P_{\max}^u), \end{aligned} \quad (\text{B.1})$$

where $\{\lambda_n, \mu_n, \nu_n\}_n^N$ are non-negative lagrange multipliers. Based on the definition of KKT conditions, we have

$$\begin{aligned} \frac{\partial \mathcal{L}}{\partial p_n^u} = & \lambda_n - \lambda_n t_n \frac{\partial R_n^a}{\partial p_n^u} - \mu_n \frac{\partial \gamma_n^a}{\partial p_n^u} + \nu_n \\ & - \sum_{j \neq n}^N \lambda_j t_j \frac{\partial R_j^a}{\partial p_n^u} - \sum_{j \neq n}^N \mu_j \frac{\partial \gamma_j^a}{\partial p_n^u} = 0, \end{aligned} \quad (\text{B.2})$$

$$\frac{\partial \mathcal{L}}{\partial t_n} = I_n - \lambda_n R_n^a = 0, \quad (\text{B.3})$$

$$\lambda_n (p_n^u - t_n R_n^a) = 0, \quad (\text{B.4})$$

$$\mu_n (\tau - \gamma_n^a) = 0, \quad (\text{B.5})$$

$$\nu_n (p_n^u - P_{\max}^u) = 0. \quad (\text{B.6})$$

In (B.2), we have $\frac{\partial R_j^a}{\partial p_n^u} = -\frac{B_a}{\ln 2} \frac{(\gamma_j^a)^2 |\mathbf{w}_j^H \mathbf{h}_{n,j}^a|^2}{p_j^u |\mathbf{w}_j^H \mathbf{h}_{j,j}^a|^2 (1 + \gamma_j^a)}$, and $\frac{\partial \gamma_j^a}{\partial p_n^u} = -\frac{(\gamma_j^a)^2 |\mathbf{w}_j^H \mathbf{h}_{n,j}^a|^2}{p_j^u |\mathbf{w}_j^H \mathbf{h}_{j,j}^a|^2}$. Based on (B.2)–(B.6), we observe that the N subproblems shown in (18) has the same KKT conditions with problem (17). In other words, problems (17) and (18) have the same optimal solution. In addition, since $R_n^a > 0$, we have $\lambda_n = \frac{I_n}{R_n^a}$ based on (B.3), and $t_n = \frac{p_n^u}{R_n^a}$ based on (B.4). Likewise, by considering the KKT conditions of N subproblems (18), we find that they are identical to those shown in (B.2)–(B.6).

APPENDIX C: PROOF OF THEOREM 1

Based on (B.2), (B.5) and (B.6) of Appendix B, KKT conditions for subproblem (18) is given by

$$\lambda_n + M_n - \frac{B_a}{\ln 2} \frac{\lambda_n t_n \Lambda_n}{1 + \gamma_n^a} - \mu_n \Lambda_n + \nu_n = 0, \quad (\text{C.1})$$

$$\mu_n (\tau - \gamma_n^a) = 0, \quad (\text{C.2})$$

$$\nu_n (p_n^u - P_{\max}^u) = 0, \quad (\text{C.3})$$

where $\Lambda_n = \frac{|\mathbf{w}_n^H \mathbf{h}_{n,n}^a|^2}{\sum_{i=1, i \neq n}^N p_i^u |\mathbf{w}_n^H \mathbf{h}_{i,n}^a|^2 + |\mathbf{w}_n^H \mathbf{h}_{n,n}^a|^2}$. From (C.1), we see that the optimal p_n^{u*} meets

$$p_n^{u*} = \frac{B_a}{\ln 2} \frac{\lambda_n t_n}{\lambda_n + M_n - \mu_n^* \Lambda_n + \nu_n^*} - \frac{1}{\Lambda_n}, \quad (\text{C.4})$$

where μ^* and ν_n^* satisfy the KKT conditions (C.2) and (C.3), respectively. To explicitly obtain $\{p_n^{u*}, \mu_n^*, \nu_n^*\}$, we need to consider the following cases:

- Case 1: When $p_n^{u*} \in \left(\frac{\tau}{\Lambda_n}, P_{\max}^u\right)$, $\mu_n^* = \nu_n^* = 0$ according to (C.2) and (C.3). In this case, $p_n^{u*} = G_n$ with $G_n = \frac{B_a}{\ln 2} \frac{\lambda_n t_n}{\lambda_n + M_n} - \frac{1}{\Lambda_n}$ according to (C.4). Therefore, if $G_n \in \left[\frac{\tau}{\Lambda_n}, P_{\max}^u\right]$, $p_n^{u*} = G_n$ and $\mu_n^* = \nu_n^* = 0$.
- Case 2: If $G_n < \frac{\tau}{\Lambda_n}$, it is seen from (C.4) that $\mu^* > 0$. In this case, $p_n^{u*} = \frac{\tau}{\Lambda_n}$ and $\nu_n^* = 0$ according to (C.2) and (C.3). Substituting $p_n^{u*} = \frac{\tau}{\Lambda_n}$ and $\nu_n^* = 0$ into (C.4), we obtain $\mu_n^* = \frac{\lambda_n + M_n}{\Lambda_n} - \frac{B_a}{\ln 2} \frac{\lambda_n t_n}{\tau + 1}$.
- Case 3: If $G_n > P_{\max}^u$, it is seen from (C.4) that $\nu_n^* > 0$. In this case, $p_n^{u*} = P_{\max}^u$ and $\mu_n^* = 0$ according to (C.3) and (C.2). Substituting $p_n^{u*} = P_{\max}^u$ and $\mu_n^* = 0$ into (C.4), we obtain $\nu_n^* = \frac{B_a}{\ln 2} \frac{\lambda_n t_n}{P_{\max}^u + 1/\Lambda_n} - \lambda_n - M_n$.

Thus, we get the optimal $\{p_n^{u*}, \mu_n^*, \nu_n^*\}$ shown in **Theorem 1**.

REFERENCES

- [1] S. Barbarossa, S. Sardellitti, and P. D. Lorenzo, “Communicating while computing: Distributed mobile cloud computing over 5G heterogeneous networks,” *IEEE Signal Process. Mag.*, vol. 31, no. 6, pp. 45–55, Nov. 2014.
- [2] Y. Mao, C. You, J. Zhang, K. Huang, and K. B. Letaief, “A survey on mobile edge computing: The communication perspective,” *IEEE Commun. Surveys & Tutorials*, vol. 19, no. 4, pp. 2322–2358, 2017.
- [3] ETSI White Paper No. 23: “Cloud RAN and MEC: A perfect pairing”, Feb. 2018.
- [4] 5GAA White Paper: “Toward fully connected vehicles: Edge computing for advanced automotive communications”, Dec. 2017.
- [5] P. Mach and Z. Becvar, “Mobile edge computing: A survey on architecture and computation offloading,” *IEEE Commun. Surveys & Tutorials*, vol. 19, no. 3, pp. 1628–1656, 2017.
- [6] M. Chiang, S. Ha, C. L. I, F. Risso, and T. Zhang, “Clarifying fog computing and networking: 10 questions and answers,” *IEEE Commun. Mag.*, vol. 55, no. 4, pp. 18–20, Apr. 2017.
- [7] K. Dolui and S. K. Datta, “Comparison of edge computing implementations: Fog computing, cloudlet and mobile edge computing,” in *Global Internet of Things Summit (GIoTS)*, 2017, pp. 1–6.
- [8] T. Verbelen, P. Simoens, F. De Turck, and B. Dhoedt, “Cloudlets: Bringing the cloud to the mobile user,” in *Proc. ACM Workshop on Mobile Cloud Computing and Services*, 2012, pp. 29–36.
- [9] ETSI White Paper No. 20: “Developing software for multi-access edge computing”, Sept. 2017.
- [10] O. Muñiz, A. Pascual-Iserte, and J. Vidal, “Optimization of radio and computational resources for energy efficiency in latency-constrained application offloading,” *IEEE Trans. Veh. Tech.*, vol. 64, no. 10, pp. 4738–4755, Oct. 2015.
- [11] X. Chen, L. Jiao, W. Li, and X. Fu, “Efficient multi-user computation offloading for mobile-edge cloud computing,” *IEEE/ACM Trans. Netw.*, vol. 24, no. 5, pp. 2795–2808, Oct. 2016.
- [12] C. You, K. Huang, H. Chae, and B. H. Kim, “Energy-efficient resource allocation for mobile-edge computation offloading,” *IEEE Trans. Wireless Commun.*, vol. 16, no. 3, pp. 1397–1411, Mar. 2017.
- [13] A. Al-Shuwaili and O. Simeone, “Energy-efficient resource allocation for mobile edge computing-based augmented reality applications,” *IEEE Wireless Commun. Lett.*, vol. 6, no. 3, pp. 398–401, June 2017.
- [14] C. Wang, C. Liang, F. R. Yu, Q. Chen, and L. Tang, “Computation offloading and resource allocation in wireless cellular networks with mobile edge computing,” *IEEE Trans. Wireless Commun.*, vol. 16, no. 8, pp. 4924–4938, Aug. 2017.
- [15] M. Chiang and T. Zhang, “Fog and IoT: An overview of research opportunities,” *IEEE Internet of Things J.*, vol. 3, no. 6, pp. 854–864, Dec. 2016.
- [16] X. Lyu, W. Ni, H. Tian, R. P. Liu, X. Wang, G. B. Giannakis, and A. Paulraj, “Optimal schedule of mobile edge computing for internet of things using partial information,” *IEEE J. Sel. Areas Commun.*, vol. 35, no. 11, pp. 2606–2615, Nov. 2017.
- [17] X. Sun and N. Ansari, “Green cloudlet network: A sustainable platform for mobile cloud computing,” *IEEE Trans. Cloud Comput.*, pp. 1–14, Early Access Articles 2017.
- [18] C. You, K. Huang, and H. Chae, “Energy efficient mobile cloud computing powered by wireless energy transfer,” *IEEE J. Sel. Areas Commun.*, vol. 34, no. 5, pp. 1757–1771, May 2016.
- [19] X. Hu, K. K. Wong, and K. Yang, “Wireless powered cooperation-assisted mobile edge computing,” *IEEE Trans. Wireless Commun.*, vol. 17, no. 4, pp. 2375–2388, Apr. 2018.
- [20] F. Wang, J. Xu, X. Wang, and S. Cui, “Joint offloading and computing optimization in wireless powered mobile-edge computing systems,” *IEEE Trans. Wireless Commun.*, vol. 17, no. 3, pp. 1784–1797, Mar. 2018.
- [21] S. Bi and Y. J. A. Zhang, “Computation rate maximization for wireless powered mobile-edge computing with binary computation offloading,” *IEEE Trans. Wireless Commun.*, pp. 1–14, Early Access Articles 2018.

- [22] Y. Yang and M. Pesavento, "A unified successive pseudoconvex approximation framework," *IEEE Trans. Signal Process.*, vol. 65, no. 13, pp. 3313–3328, July 2017.
- [23] A. Zappone and E. Jorswieck, *Energy Efficiency in Wireless Networks via Fractional Programming Theory*. Now Foundations and Trends, 2015, vol. 11, no. 3-4.
- [24] E. Björnson, E. G. Larsson, and T. L. Marzetta, "Massive MIMO: ten myths and one critical question," *IEEE Commun. Mag.*, vol. 54, no. 2, pp. 114–123, Feb. 2016.
- [25] H. Q. Ngo, and E. G. Larsson, "No downlink pilots are needed in TDD massive MIMO," *IEEE Trans. Wireless Commun.*, vol. 16, no. 5, pp. 2921–2935, May 2017.
- [26] P. Harris, S. Malkowsky, J. Vieira, E. Bengtsson, F. Tufvesson, W. B. Hasan, L. Liu, M. Beach, S. Armour, and O. Edfors, "Performance characterization of a real-time massive MIMO system with LOS mobile channels," *IEEE J. Sel. Areas Commun.*, vol. 35, no. 6, pp. 1244–1253, Apr. 2017.
- [27] T. L. Marzetta, "Noncooperative cellular wireless with unlimited numbers of base station antennas," *IEEE Trans. Wireless Commun.*, vol. 9, no. 11, pp. 3590–3600, Nov. 2010.
- [28] H. Q. Ngo, E. G. Larsson, and T. L. Marzetta, "Energy and spectral efficiency of very large multiuser MIMO systems," *IEEE Trans. Commun.*, vol. 61, no. 4, pp. 1436–1449, Apr. 2013.
- [29] A. He, L. Wang, Y. Chen, K. K. Wong, and M. Elkashlan, "Spectral and energy efficiency of uplink D2D underlaid massive MIMO cellular networks," *IEEE Trans. Commun.*, vol. 65, no. 9, pp. 3780–3793, Sept. 2017.
- [30] 3GPP TR 36.814 v9.2.0, "3rd generation partnership project: technical specification group radio access network: Evolved universal terrestrial radio access (E-UTRA): further advancements for E-UTRA physical layer aspects," Mar. 2017.